ANALYTIC METHOD TO IDENTIFY TRAIN LOAD FROM INTEGRATED SLEEPER IN-SITU

Le Hung Tran, Tien Hoang, Denis Duhamel, Gilles Forêt, S Messad, A Loaec

13th World Congress on Computational Mechanics (WCCM XIII)
2nd Pan American Congress on Computational Mechanics (PANACM II)
July 22–27, 2018, New York City, NY, USA

ANALYTIC METHOD TO IDENTIFY TRAIN LOAD FROM INTEGRATED SLEEPER IN-SITU

L-H. TRAN[*†], T. HOANG[*], D. DUHAMEL[*], G. FORET[*], S. MESSAD[†] AND A. LOAËC[†]

[*]Laboratoire Navier, UMR 8205, Ecole des Ponts ParisTech,
IFSTTAR, CNRS, UPE, Champs-sur-Marne, France
le-hung.tran@enpc.fr, tien.hoang@enpc.fr, denis.duhamel@enpc.fr, gilles.foret@enpc.fr

[†]SATEBA, 33 places des Corolles, 92400 Courbevoie, France
s.messad@sateba.com, a.loaec@sateba.com

Key words: Railway Dynamics, Instrumented Sleeper, Fiber Bragg gratings, Green's function, Computation methods.

Abstract. The degradation of railway tracks can be observed through several measurement techniques. Recently, a method to diagnose the railway track using Fiber Bragg gratings (FBG) has been proposed. FBG are integrated inside the railway sleeper and is named a "Smart Sleeper". To study the sleeper behavior, an analytical model for the dynamics of railway sleepers has been developed, which can calculate rapidly the sleeper responses. In this model, by using the relation between the rail forces and displacements of a periodically supported beam, the dynamic equation of the sleeper is written with the help of the Euler-Bernoulli beam equation and Dirac's functions. Subsequently, thanks to the Green's function of this system, the sleeper dynamic response is calculated analytically. A linear relation between the train loads and the sleeper strains is shown in the frequency domain. This article presents an application of this model to calculate the train loads from the strains measured by the FBG. Based on the analytical model, we obtain a matrix which presents the link between the loads and the sleeper responses. By integrating this matrix and the Fourier transform of the measurements recorded by the FBG at the middle and at the two rail-seats, the train loads can be quickly calculated by using the solver `mldivide` of MATLAB. The numerical application shows that the identified train loads are different for different wheels and different rails. This highlights the irregularity of the wheel-rail contact forces which can be used to detect the defaults in the rolling stock in future works.

1 INTRODUCTION

Generally, defective materials can be detected by several different methods. The easiest is the correlation by image analysis but it is slow and not exact. Measurement of elastic waves, electrical resistance or acoustic emission focus on a variation of the propagation time of waves and electrical resistance to detect the internal cracks of objects. The study of the dynamic properties of systems in the frequency domain (modal analysis) is then applied [1, 2, 3]. Material

damage would have abnormal resonant frequencies.

In recent years, a novel technology using the Fiber Bragg Grating (FBG) to diagnose the railway track has been developed. In 2010, Filograno et al. [12] posed the FBG sensors on the rail in different directions (vertical, horizontal and inclined at an angle 45°) for monitoring the high speed line from Madrid to Barcelona in real time. They could detect the train parameters: train speed and acceleration, the distance between the wheel and wheel number. Moreover, the dynamic charge can be calculated in a precise way. Wei et al. [13, 14] presented two methods: X-Crossing and D-Crossing to avoid the area where signals are noisy. Buggy et al. [15] has used the FBG to monitor the fishplate (jonction of two rails). In the same year, Tam et al. [16] presented the system "Smart Railways" which has been developped by KCRS's East Rail in Hong Kong. The FBG sensor has been demonstrated to be able to detect the rail imperfection [17, 18]. A railway sleeper "Smart Sleeper" [19] which has been developed by Sateba with 6 sensors allows us to measure the sleeper strain when the train is passing.

Substantial research using analytical and numerical methods for rail track has been carried out. Analytical models of the rail track have been developped by considering the model of an infinite beam placed on a continuous foundation [8, 9, 10] or a periodically supported beam [4, 5, 6, 7]. Some research focus on the pre-stressed concrete sleeper using FEM in 2D and in 3D [20, 21]. In 2017, Tran et al. [11] has developped an analytical model of the railway sleeper which allows us to rapidly calculate the sleeper response.

In this paper, based on the analytical model of the railway sleeper, an "inverse problem" has been developped to determine the train loads. By considering a beam resting on a Kelvin-Voigt foundation and by assuming a periodic charge, the sleeper strain and the train loads can be written as a linear relation in the frequency domain with the help of the Green's function. The charges can be determined by using the MATLAB solver `mldivide`. We verified this problem to a good precision by back-calculating the train loads from a signal. That is a combination of imposed loads and random noise. Another application has been shown in this paper with the real measurements recorded by the "Smart Sleeper". The results of this application shows the differents charges applied on each rail which corresponds to different strain level recorded by the FGB of the sleeper.

2 GORVERNING EQUATIONS

2.1 Analytical model of the sleeper

A railway track can be modeled as shown in Fig. 1. In this track, the sleeper together with the ballast and foundation are modeled by an Euler-Bernouilli beam resting on a Kelvin-Voigt foundation. The sleeper length is $2L$ (from $-L$ to L) and the rail positions are at $x = \pm a$. The sleeper displacement $w_s(x,t)$ under a force $F(x,t)$ is driven by the dynamic equation of the Euler-Bernoulli pre-stressed beam as follows:

$$E_s I_s \frac{\partial^4 w_s(x,t)}{\partial x^4} + \rho_s S_s \frac{\partial^2 w_s(x,t)}{\partial t^2} - T\frac{\partial^2 w_s(x,t)}{\partial x^2} + k_f w_s(x,t) + \zeta_f \frac{\partial w_s(x,t)}{\partial t} = F(x,t) \quad (1)$$

where ρ_s, E_s, S_s and I_s are the density, the Young's modulus, the section and the cross-sectional moment inertia of the sleeper respectively; k_f and ζ_f are the stiffness and damping coefficients

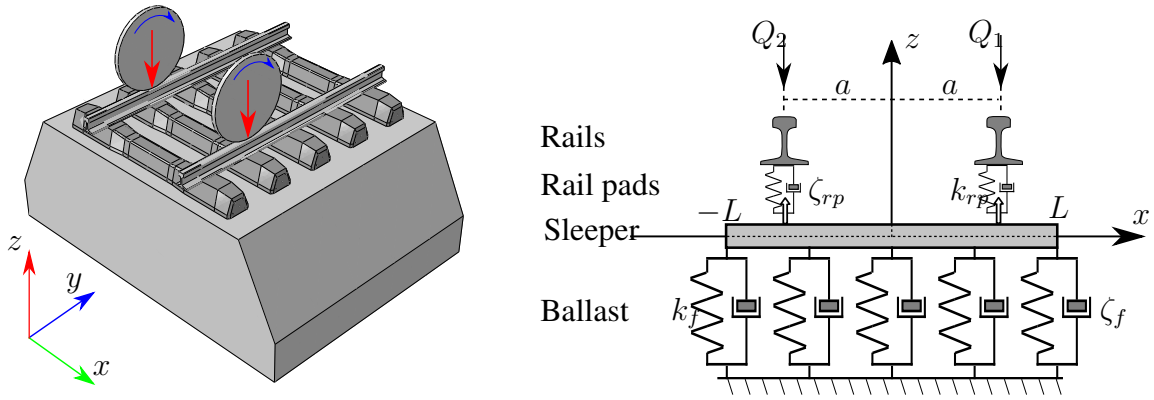

(a) (b)

Figure 1: Railway track (a) and the analytical model representation (b)

of the foundation and T is the sleeper pre-stress. The force applied by the rails on the sleeper $F(x,t)$ can be written with the help of the Dirac's functions as follows :

$$F(x,t) = -R_1(t)\delta(x-a) - R_2\delta(x+a) \tag{2}$$

where R_1 and R_2 are the reaction forces applied on the rail positions ($x = \pm a$). For a free-free beam posed on the foundation, the moment (3a) and the shear force (3b) are vanishing at two extremities, thus these boundary conditions can be imposed by the 2^{nd} and 3^{rd} partial derivative with regard to x set to zero respectively:

$$\begin{cases} \dfrac{\partial^2 w_s}{\partial x^2}(-L,t) = \dfrac{\partial^2 w_s}{\partial x^2}(L,t) = 0 & \text{(3a)} \\ \dfrac{\partial^3 w_s}{\partial x^3}(-L,t) = \dfrac{\partial^3 w_s}{\partial x^3}(L,t) = 0 & \text{(3b)} \end{cases}$$

Eq. (1) together with the boundary conditions (3) is a 4^{th} order linear differential equation in the frequency domain which can be solved with help of the Green's function. (The calculation of the Green's function is shown in Appendix B). Hence, the sleeper response in the frequency domain $\hat{w}_s(x,\omega)$ can be written as follow:

$$\hat{w}_s(x,\omega) = \frac{-\hat{R}_1}{E_s I_s} G_a(x,\omega) + \frac{-\hat{R}_2}{E_s I_s} G_{-a}(x,\omega) \tag{4}$$

By substituting $x = a$ and $x = -a$ into the aforementioned equation, we obtain respectively the sleeper displacement at the rail positions:

$$\begin{aligned} \hat{w}_s(a,\omega) &= \frac{-\hat{R}_1}{E_s I_s} G_a(a,\omega) + \frac{-\hat{R}_2}{E_s I_s} G_{-a}(a,\omega) \\ \hat{w}_s(-a,\omega) &= \frac{-\hat{R}_1}{E_s I_s} G_a(-a,\omega) + \frac{-\hat{R}_2}{E_s I_s} G_{-a}(-a,\omega) \end{aligned} \tag{5}$$

The model of the periodically supported beam and together with the consecutive law of the rail pads shows the expression of the reaction force (see Appendix A). The combination at Eqs. (17) and (5) gives us the result of the reaction force of the sleeper on the two rails:

$$\begin{aligned}\hat{R}_1 &= \frac{E_s I_s}{\mathcal{K}} \frac{\mathcal{Q}_1 \left[G_{-a}(-a,\omega)+\chi\right] - \mathcal{Q}_2 G_{-a}(a,\omega)}{\left[\chi+G_a(a,\omega)\right]\left[\chi+G_{-a}(-a,\omega)\right] - G_a(-a,\omega)G_{-a}(a,\omega)} \\ \hat{R}_2 &= \frac{E_s I_s}{\mathcal{K}} \frac{\mathcal{Q}_2 \left[G_a(a,\omega)+\chi\right] - \mathcal{Q}_1 G_a(-a,\omega)}{\left[\chi+G_a(a,\omega)\right]\left[\chi+G_{-a}(-a,\omega)\right] - G_a(-a,\omega)G_{-a}(a,\omega)}\end{aligned} \tag{6}$$

where $\chi = E_s I_s \dfrac{k_p + \mathcal{K}}{k_p \mathcal{K}}$. Then, the sleeper displacement in the frequency domain can be obtained by replacing $\hat{R}_1$ and $\hat{R}_2$ in Eq. (4). The sleeper strain can be calculated using the beam theory and together with the equation of the sleeper response (4):

$$\hat{\varepsilon}_x(x,z,\omega) = z_s \left(\frac{\hat{R}_1}{E_s I_s} G_a''(x,\omega) + \frac{\hat{R}_2}{E_s I_s} G_{-a}''(x,\omega) \right) \tag{7}$$

where z_s is the distance to the beam's neutral axis. By using the inverse Fourier transform of Eqs. (4) and (7), we can get the sleeper response and the sleeper strain in the time domain.

2.2 Identifcation of the train load

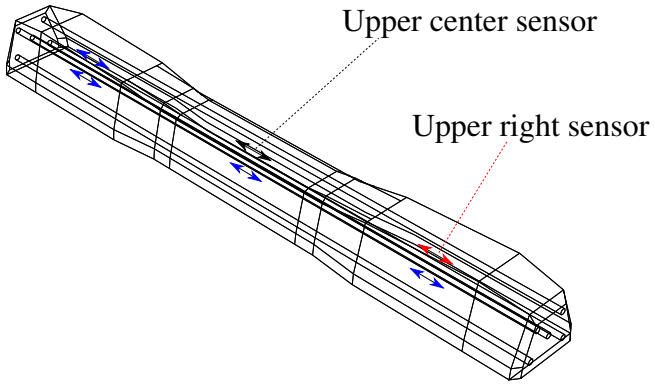

Figure 2: Instrumented sleeper: upper right sensor (red), and uper center sensor (black)

We will apply this analytical model to identify the train load from the sleeper strain. A "Smart Sleeper" which has been developped by Sateba with 6 Fibre Bragg Grating sensors (FBG) integrated in the longitudinal direction allow us to obtain the sleeper strain as the train passes. These sensors are situated at the two rail seats and at the middle of the sleeper. The signals are recorded by these sensors in the time domain and by using the Fourier transform, we can obtain these signals in the frequency domain. We can rewrite Eq. (7) as follows:

$$\hat{\varepsilon}_i(x_i, z_{s_i}, \omega) = \mathbf{A_{i1}}(x_i, z_{s_i}, \omega)\hat{R}_1(\omega) + \mathbf{A_{i2}}(x_i, z_{s_i}, \omega)\hat{R}_2(\omega) \tag{8}$$

where (x_i, z_{s_i}) are the positions of the sensors, $\mathbf{A_{i1}} = \left(\frac{z_{s_i}}{E_s I_s} G''_a(x_i, \omega)\right)$ and $\mathbf{A_{i2}} = \left(\frac{z_{s_i}}{E_s I_s} G''_{-a}(x_i, \omega)\right)$. This equation can be also rewritten as:

$$\left[\hat{\varepsilon}(\omega)\right] = \begin{bmatrix}\mathbf{A_{i1}}(\omega) & \mathbf{A_{i2}}(\omega)\end{bmatrix} \begin{bmatrix}\hat{R}_1(\omega) \\ \hat{R}_2(\omega)\end{bmatrix} \tag{9}$$

where $\left[\hat{\varepsilon}(\omega)\right]$ represents the vector signals in the frequency domain and has a dimension n_f that depends on the number of signals.

The reaction forces of the sleeper on the rail can be calculated by the equivalent charges $\mathcal{Q}_k$ where $k = 1, 2$ which corresponds to right and left rails. From Eq. (6), we obtain:

$$\begin{bmatrix}\hat{R}_1(\omega) \\ \hat{R}_2(\omega)\end{bmatrix} = \begin{bmatrix}\mathbf{B_{11}}(\omega) & \mathbf{B_{12}}(\omega) \\ \mathbf{B_{21}}(\omega) & \mathbf{B_{22}}(\omega)\end{bmatrix} \begin{bmatrix}\mathcal{Q}_1(\omega) \\ \mathcal{Q}_2(\omega)\end{bmatrix} \tag{10}$$

where these 4 components $\mathbf{B_{ik}}$ are 4 known constants. The equivalent charges $\mathcal{Q}_k$ are calculated on each rail k (see Appendix A) as follows:

$$\mathcal{Q}_k(\omega) = \frac{\mathcal{K}(\omega)}{v E_r I_r \left[\left(\frac{\omega}{v}\right)^4 - \lambda_r^4\right]} \sum_{j=1}^{K} Q_{kj} \mathrm{e}^{-\mathrm{i}\omega \frac{D_j}{v}} = \left[\mathbf{C}(\omega)\right] \mathbf{Q_k} \tag{11}$$

where $\mathbf{Q_k} = \left[Q_{kj}\right]_j$ is a column vector of all moving loads on the rail k. The matrix $\left[\mathbf{C}(\omega)\right]$ has dimensions $[n_f \times K]$ with n_f and K represent the length of the vector $\left[\hat{\varepsilon}(\omega)\right]$ and the wheel number respectively. Eq. (11) can be rewritten as follows:

$$\begin{bmatrix}\mathcal{Q}_1(\omega) \\ \mathcal{Q}_2(\omega)\end{bmatrix} = \left[\mathbf{C}(\omega)\right] \begin{bmatrix}\mathbf{Q_1} \\ \mathbf{Q_2}\end{bmatrix} \tag{12}$$

The combination of Eqs. (9), (10), and (12) allows us to deduce the relation between the sleeper strains and the train loads as follows:

$$\left[\hat{\varepsilon}(\omega)\right] = \begin{bmatrix}\mathbf{A_{i1}}(\omega) & \mathbf{A_{i2}}(\omega)\end{bmatrix} \begin{bmatrix}\mathbf{B_{11}}(\omega) & \mathbf{B_{22}}(\omega) \\ \mathbf{B_{21}}(\omega) & \mathbf{B_{22}}(\omega)\end{bmatrix} \left[\mathbf{C}(\omega)\right] \begin{bmatrix}\mathbf{Q_1} \\ \mathbf{Q_2}\end{bmatrix} \tag{13}$$

And we can also rewritten the Eq. (13) as a linear equation:

$$\left[\hat{\varepsilon}(\omega)\right] = \begin{bmatrix}\mathbf{F_{i1}}(\omega) & \mathbf{F_{i2}}(\omega)\end{bmatrix} \begin{bmatrix}\mathbf{Q_1} \\ \mathbf{Q_2}\end{bmatrix} = \left[\mathbf{F}(\omega)\right] \left[\mathbf{Q}\right] \tag{14}$$

Eq. (14) is a linear relation between the sleeper strains and train loads. Hence, we can use function `mldivide`[1] in MATLAB to solve this linear equation.

[1]This solver has many methods of factorization to solve a system linear equation which depend on the dimension of the matrices (for example: Cholesky factorization for a matrix symmetric with real, positive diagonal element; Gaussian elimination to reduce the system to a triangular matrix if the matrix is upper Hessenberg etc.). In this case, the matrix $\mathbf{F}(\omega)$ is rectangular, thus method of QR factorization will be used in the `mldivide` solver

3 NUMERICAL APPLICATION

3.1 Verification

The objective of this section is to verify the precision of the inverse problem. By using the analytical signals generated by the analytical model, we apply it on the inverse problem to identify the train loads. The test will be done with the analytical signal and noise signal. The parameters of the railway track is shown in Table 1. These parameters allows us to generate the analytical signals for identifying the train loads.

Content	Unit	Notation	Value
Young's modulus of rail	GPa	E_r	210
Cross-sectional moment inertia of rail	m^4	I_r	3E-05
Rail density	kgm^{-3}	ρ_r	7850
Rail section area	m^2	S_r	7.69E-3
Young's modulus of sleeper	GPa	E_s	48
Cross-sectional moment inertia of sleeper	m^4	I_s	4.32E-4
Density of sleeper	kgm^{-3}	ρ_s	2475
Sleeper section area	m^2	S_s	54.9E-3
Length of sleeper	m	$2L$	2.41
Track gauge	m	$2a$	1.435
Stiffness of ballast	MNm^{-1}	k_f	240
Damping coefficient of ballast	$kNsm^{-1}$	ζ_f	58.8
Stiffness of rail pad	MNm^{-1}	k_{rp}	192
Damping coefficient of rail pad	$MNsm^{-1}$	ζ_{rp}	1.97
Train speed	ms^{-1}	v	50
Pre-stress of sleeper	kN	T	300
Sleeper spacing	m	l	0.6

Table 1: Parameters of the railway track

The charge per wheel on each rail has been generated randomly. Fig. 3 shows the superposition of the charges introduced and indentified (blue line and red column respectively) on the left rail (a) and right rail(b). In the two figures, the blue line has the same value as the red columns in this figure because we found the same train loads. The relative error is about 3.7×10^{-4} %. We can conclude that the inverse problem is verified with a good precision. The difference is due to small errors introduced during the numerical calcultations.

Now, we add a random noise to the sleeper response to simulate the real measurments. Fig. 4 shows the sleeper strain as a red line and the noise signal as a blue line on the left rail (a) and right rail (b) in a time interval which corresponds to the time for the passing of a train. By using the inverse problem, the superposition of the train loads introduced and identified is shown in Fig. 5.

With the noise, the train loads have been found with a small difference. In this figure, the red column and blue line corresponding to trains loads introduced and identified don't have the same value. The table 2 shows the relative error with different levels of noise in the signal.

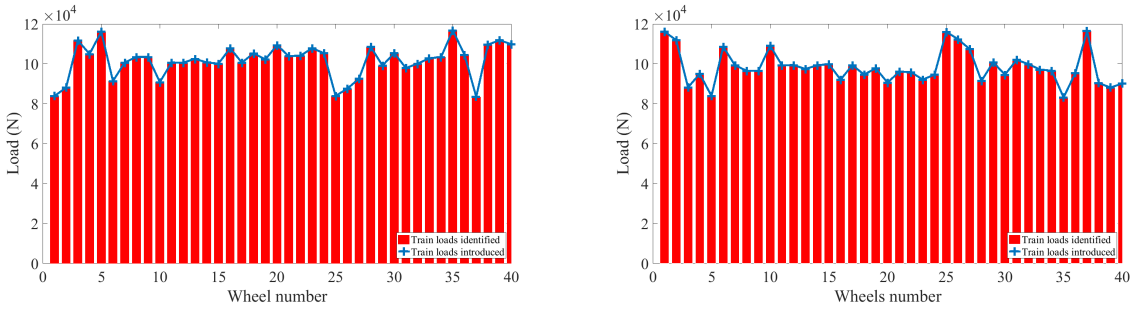

(a) Left rail (b) Right rail

Figure 3: Superposition of the train loads introduced and identified on the left rail (a) and right rail (b)

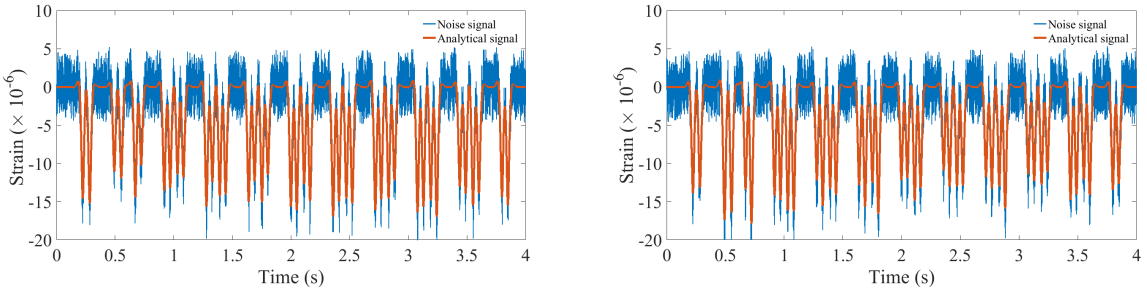

(a) Left rail (b) Right rail

Figure 4: Analytical and noise signals on the left rail (a) and right rail (b)

Amplitude of noise	Left rail	Right rail	Average
Slightly noisy	0.281 %	0.285 %	0.283 %
Noisy	0.585 %	0.597 %	0.592 %
Very noisy	1.186 %	1.159 %	1.172 %
Strongly noisy	2.541 %	2.634 %	2.588 %

Table 2: Relative error between the train loads introduced and identified fore different noise levels

Fig. 4 shows the case of large amount of introduced noise which the relative error is 1.17 %. With the strongly noisy signal, the relative error is about 2.6 %. Thus, we can conclude that the train loads identified have been found with a good precision.

3.2 Real signal

We will use the measurements recorded in-situ with the help of the "Smart Sleeper". The measurement has been performed at Creil, France, on the 6^{th} of May 2017. Fig. 7 shows the signal recorded by the "Smart Sleeper" during the passing of a train which contains 10 wagons

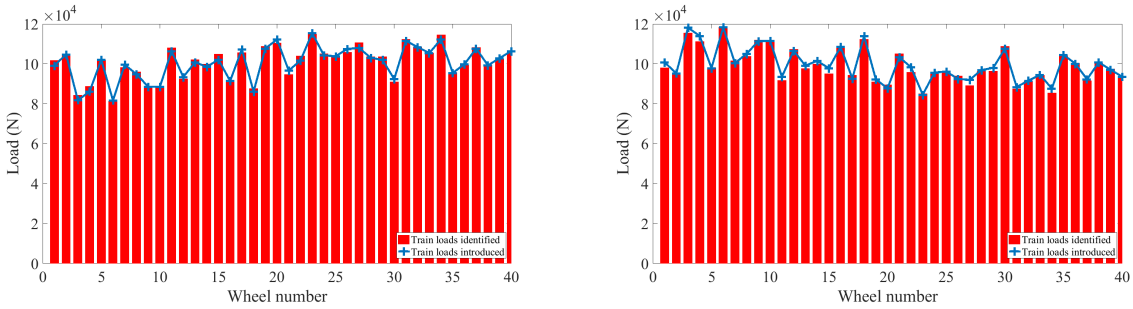

(a) Left rail (b) Right rail

Figure 5: Superposition of the train loads introduced and identified on the left rail (a) and right rail (b)

including the locomotive. The green and red line represent the measurements on the left (a) and right (b) upper sensor respectively. The train loads on the two rails are shown in Fig. 6. The black in Fig. 7 represents the analytical sleeper response by using the identified train loads.

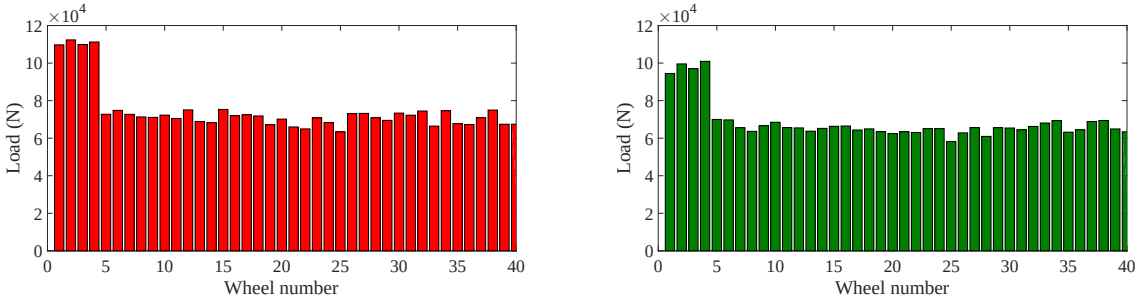

(a) Left rail (b) Right rail

Figure 6: Train loads identified by using the measurements on the left rail (a) and right rail (b)

We note that the value of the first four loads on the two rails are bigger than the rest, corresponding to the locomotive of the train, which is normally heavier than the wagons. In the Fig. 7, the first four peaks are also superior to the rest.

Moreover, we note that the train loads on the two rails are not the same (in Fig 7, the sleeper strains on the left rail are superior to the right rail). By identifying the train loads, this phenomenon is demonstrated by the different charges on the two rails. The charges applied on the left rail are bigger than the right rail. This could be explained by the non-homogenous foundation or by the unbalanced of rolling stock.

4 CONCLUSION

Based on an analyical model of the railway sleeper the inverse problem has been developed to identify the train loads. In the frequency domain, the sleeper strain and the train loads can be linked by a linear relation. The train loads identified from the measurements in-situ demonstrate

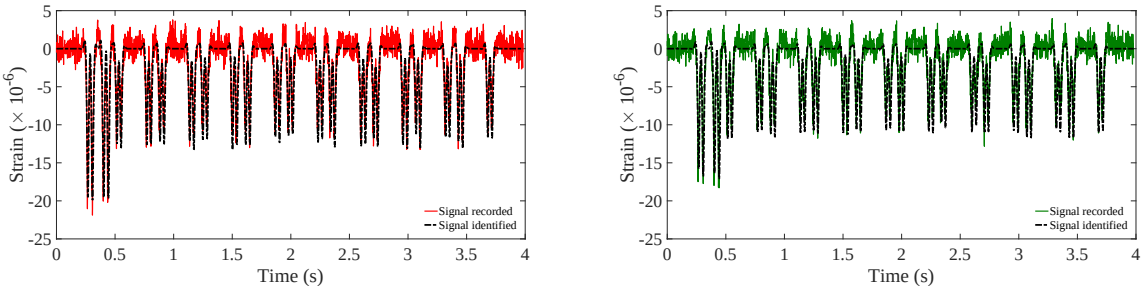

(a) Upper left sensor

(b) Upper right sensor

Figure 7: Sleeper response on the left rail (a) and right rail (b)

different values for each wheel of the train. Thus, this technique can detect the imperfection of the wheel-rail contact when the train load on one rail is much higher than the other. In future works, the model should be developed to identify other parameters of the railway track.

Acknowledgement

This work has been developped in the context of a partnership between Sateba (Consolis Group) and Ecole des Ponts ParisTech. The authors would like to thank the personnel of Sateba for their support.

A Periodically supported beam model

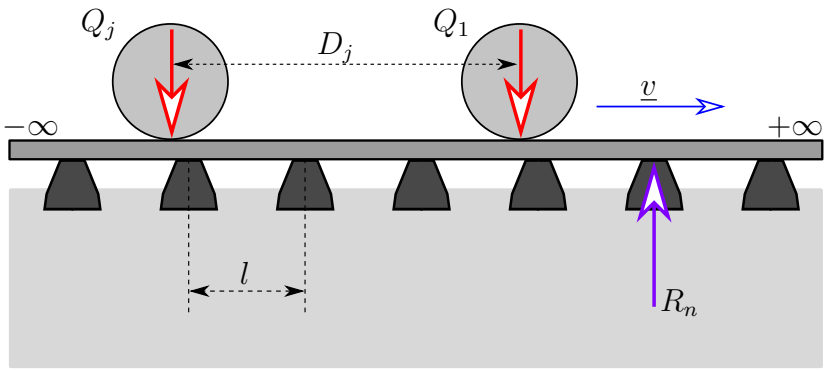

Figure 8

The periodically supported beam is shown in Fig. 8. When the rails are modeled by periodically supported beams [7], the forces R_k on each rail k in the frequency domain can be calculated as follows:

$$\hat{R}_k(\omega) = \mathcal{K}\hat{w}_r^{(k)}(\omega) + \mathcal{Q}_k(\omega) \tag{15}$$

where $\mathcal{K}$ is the equivalent stiffness, $\mathcal{Q}_k$ are the equivalent charges of the two rails which are determined. Let $w_r^{(k)}$ be the rail k displacements at the sleeper position respectively and $w_s(x,t)$

is the sleeper displacement where $x = \pm a$ corresponds to the positions of the rail seats. The forces $\hat{R}_k$ can be expressed by the constitutive law of the rail pads in the frequency domain as follows:

$$\hat{R}_k(\omega) = -k_p \left(\hat{w}_r^{(k)}(\omega) - \hat{w}_s(a,\omega) \right) \tag{16}$$

where $k_p = k_{rp} + \mathrm{i}\omega\zeta_{rp}$ is the dynamic stiffness of the rail pad and k_{rp}, ζ_{rp} are the stiffness and damping coefficients of the rail pads. By substituting Eq. (15) into Eq. (16), we obtain:

$$\hat{R}_k(\omega) = \frac{k_p \mathcal{K}}{k_p + \mathcal{K}} \hat{w}_s(a,\omega) + \frac{k_p}{k_p + \mathcal{K}} \mathcal{Q}_k(\omega) \tag{17}$$

B Green's function

By using the Fourier transform and combining equations (1), (2) and (3), this system dynamics equation can be rewritten in the frequency domain :

$$\begin{cases} \hat{w}_s''''(x,\omega) - \dfrac{T}{E_s I_s} \hat{w}_s''(x,\omega) - \dfrac{\rho_s S_s \omega^2 - k_b}{E_s I_s} \hat{w}_s(x,\omega) = -\dfrac{\hat{R}_1}{E_s I_s} \delta(x-a) - \dfrac{\hat{R}_2}{E_s I_s} \delta(x+a) \\ \hat{w}_s''(-L,\omega) = \hat{w}_s''(L,\omega) = 0 \\ \hat{w}_s'''(-L,\omega) = \hat{w}_s'''(L,\omega) = 0 \end{cases} \tag{18}$$

where $\left(\square'\right)$ stands for the partial derivative with regard to x and $k_b = k_f + \mathrm{i}\omega\zeta_f$ is the foundation dynamic stiffness. The Green's function $G_a(x,\omega)$ of Eq. (18) is defined by :

$$\frac{\partial^4 G_a(x,\omega)}{\partial x^4} - \alpha_s^2 \frac{\partial^2 G_a(x,\omega)}{\partial x^2} - \lambda_s^4 G_a(x,\omega) = \delta(x-a) \tag{19}$$

where $\alpha_s = \sqrt{\dfrac{T}{E_s I_s}}$ and $\lambda_s = \sqrt[4]{\dfrac{\rho_s S_s \omega^2 - k_b}{E_s I_s}}$. This is a 4^{th} order linear differential equation and its Green's function [22] can be written as follows:

$$G_a(x,\omega) = \begin{cases} A_1 \mathrm{e}^{\lambda_1 x} + A_2 \mathrm{e}^{\lambda_2 x} + A_3 \mathrm{e}^{\lambda_3 x} + A_4 \mathrm{e}^{\lambda_4 x} & \text{for } x \in [-L, a] \\ B_1 \mathrm{e}^{\lambda_1 x} + B_2 \mathrm{e}^{\lambda_2 x} + B_3 \mathrm{e}^{\lambda_3 x} + B_4 \mathrm{e}^{\lambda_4 x} & \text{for } x \in [a, L] \end{cases} \tag{20}$$

where A_i, B_i, and λ_i (with $1 \leq i \leq 4$) are parameters to be determined. λ_i is the 4 complex roots of the characteristic equation:

$$\mathcal{P}(\lambda) = \lambda^4 - \alpha_s^2 \lambda^2 - \lambda_s^4 \tag{21}$$

By using the boundary conditions of the free-free beam (continuity condition for displacement, slope and moments, discontinuity of magnitude one at the point force), we can obtain analytical expressions for A_i, B_i.

REFERENCES

[1] H. F. Lam, Q. Hu and M. T. Wong, The Bayesian methodology for the detection of railway ballast damage under a concrete sleeper, Engineering Structures 81 (2005) 289–301.

[2] A. Remennikov, S. Kaewunruen, Experimental Investigation on dynamic railway sleeper/ballast interaction, Experimental Mechanics 46 (1) (2006) 57–66.

[3] M. Kodai, W. Tsutomu and S. Masamichi, Damage detection method for sleepers based on vibration properties, EDP Sciences 24 (2015).

[4] D.J. Mead, Free wave propagation in periodically supported, infinite beams, Journal of Sound and Vibration 11 (2) (1970) 181–197.

[5] D.J. Mead, Wave propagation in continuous periodic structures: research contributions from Southampton, Journal of Sound and Vibration 190 (3) (1996) 495–524.

[6] X. Sheng, C. Jones and D. Thompson, Responses of infinite periodic structures to moving or stationary harmonic loads, Journal of Sound and Vibration 303 (3-5) (2007) 873–894.

[7] T. Hoang, D. Duhamel, G. Foret, H. Yin, P. Joyez and R. Caby, Calculation of force distribution for a periodically supported beam subjected to moving loads, Journal of Sound and Vibration 388 (2017) 327–338.

[8] H. Ding, L. Q. Chen, S. P. Yang, Convergence of Galerkin truncation for dynamic response of finite beams on nonlinear foundations under a moving load, Journal of Sound and Vibration 331 (10) (2012) 2426-2442.

[9] V. H. Nguyen, D. Duhamel, Finite element procedures for nonlinear structures in moving coordinate. Part 1: Infinite bar under moving axial loads, Computer & Structures 84(21) (2006) 1368–1380.

[10] V. H. Nguyen, D. Duhamel, Finite element procedures for nonlinear structures in moving coordinate. Part 2: Infinite beam under moving harmonic loads, Computer & Structures 86(21) 2056–2063.

[11] L. H. Tran, T. Hoang, D. Duhamel, G. Foret, S. Messad, A. Loaëc, Analytical model of the dynamics of railway sleeper, 6^{th} International Conference on Computational Methods in Structural Dynamics and Earthquake Engineering 2 (2017) 3937–3948.

[12] M. L. Filograno et al., Real time monitoring of railway traffic using Fiber Bragg Grating sensors, IEEE Sensors Journal 12(1) (2012) 85–92.

[13] C. Wei et al., A Fiber Bragg Grating sensor system for train axle couting, IEEE Sensors Journal 12(10) (2010) 1905–1912.

[14] C. Wei et al., Real-Time train wheel condition monitoring by Fiber Bragg Grating sensors, International Journal of Distributed Sensor Networks 10 (2012).

[15] S. J. Buggy et al., Railway track component condition monitoring using optical fibre Bragg Grating sensors, Measurements Science and Technology 27(5) (2016) 1–15.

[16] H. Y. Tam et al., Utilization of fiber optic Bragg Grating sensing systems for health monitoring in railway applications, 6^{th} International Workshop on Structural Health Monitoring, Stanford University, Stanford, CA, September 11-13, (2007) 1824.

[17] R. Pimentel et al., Hybrid Fiber-Optic/Electrical measurement system for characterization of railway traffic and its effects on a short span bridge, IEEE Sensors Journal 8(7) (2008) 1243–1249.

[18] S. L. Ho et al., Real time monitoring of railway traffic using Fiber Bragg Grating sensors, IEEE Sensors Journal (2006) 125–129.

[19] L. Arnaud, P. Charles, Smart Sleeper : Measurement of bending moments in concrete sleepers laid on ballast tracks, Transport Research Arena (TRA) 5^{th} Conference: Transport Solutions from Research to Deployment, (2014).

[20] G. Kumaran, D. Menon and K. Krishnan Nair, Dynamic studies of railtrack sleepers in a track structure system, Journal of Sound and Vibration, 268(3) (2003) 485–501

[21] A. A. Arab, S. S. Badie and M. T. Manzari, A methodological approach for finite element modeling of pretensioned concrete members at the release of pretensioning, Engineering Structures, 33(6) (2011) 1918–1929

[22] E. Zauderer, Partial differential equations of applied mathematics, John Wiley Sons (1989).